Research Square

Preprints are preliminary reports that have not undergone peer review.
They should not be considered conclusive, used to inform clinical practice,
or referenced by the media as validated information.

Ocean memory amplifies Antarctica's sea-level contribution after climate overshoot

Chen Zhao

chen.zhao@utas.edu.au

Institute for Marine and Antarctic Studies, University of Tasmania https://orcid.org/0000-0003-0368-1334

Rupert Gladstone

University of Lapland https://orcid.org/0000-0002-1582-3857

Thomas Zwinger

CSC - IT Center for Science Ltd https://orcid.org/0000-0003-3360-4401

Eliot Jager

Institute for Atmospheric and Earth System Research, University of Helsinki https://orcid.org/0000-0002-6493-0122

David Gwyther

University of Tasmania https://orcid.org/0000-0002-7218-2785

Matt King

University of Tasmania https://orcid.org/0000-0001-5611-9498

Chris R Stokes

Durham University https://orcid.org/0000-0003-3355-1573

Benjamin Galton-Fenzi

Australian Antarctic Division https://orcid.org/0000-0003-1404-4103

Poul Christoffersen

University of Tasmania https://orcid.org/0000-0003-2643-8724

Article

Keywords:

Posted Date: October 22nd, 2026

DOI: https://doi.org/10.21203/rs.3.rs-11300906/v1

License: This work is licensed under a Creative Commons Attribution 4.0 International License.
Read Full License

Additional Declarations: There is **NO** Competing Interest.

Ocean memory amplifies Antarctica's sea-level contribution after climate overshoot

Chen Zhao[*1,2,3], **Rupert Gladstone**[4], **Thomas Zwinger**[5], **Eliot Jager**[6], **David Gwyther**[3,7], **Matt A. King**[1,2,8], **Chris R. Stokes**[9], **Benjamin K. Galton-Fenzi**[7,3,2], **and Poul Christoffersen**[1,2]

[1]Institute for Marine and Antarctic Studies, University of Tasmania, Hobart, Australia
[2]Australian Centre for Excellence in Antarctic Science, University of Tasmania, Hobart, Australia
[3]Australian Antarctic Program Partnership, Institute for Marine and Antarctic Studies, University of Tasmania, Hobart, Australia
[4]Arctic Centre, University of Lapland, Rovaniemi, Finland
[5]CSC-IT Center for Science, Espoo, Finland
[6]Institute for Atmospheric and Earth System Research, University of Helsinki, Finland
[7]Australian Antarctic Division, Hobart, Australia
[8]School of Geography, Planning, and Spatial Sciences, University of Tasmania, Hobart, Australia
[9]Department of Geography, Durham University, Durham, UK
[*]chen.zhao@utas.edu.au

ABSTRACT

Exceeding the 1.5 ℃ Paris Agreement limit is now unavoidable, raising a critical question: how does the overshoot duration affect Antarctica's contribution to sea-level rise? Here we use an ice-sheet model to compare scenarios in which high-emissions forcing (SSP3-7.0) persists for 20, 50, 75 or 100 years before returning towards a low-emissions pathway (SSP1-2.6). When atmospheric and ocean forcing recover together, the additional contribution relative to sustained low forcing remains below 3 mm sea-level equivalent (SLE) by 2300 after 20–50 years of high forcing, but increases nonlinearly to 8.6 and 21.5 mm SLE after 75 and 100 years, respectively. When atmospheric and ocean forcing both recover after 50 years of high forcing, the additional contribution is only 2.3 mm SLE. However, this contribution increases to 44.1 mm SLE when ocean forcing is kept high for a further 50 years, in line with expectations of delayed ocean recovery, even while atmospheric forcing declines. Thus, shortening the overshoot duration limits Antarctica's additional contribution to sea-level rise, but the benefit depends strongly on how quickly ocean temperature declines.

Introduction

Limiting global warming to 1.5 °C above pre-industrial levels is a central goal of the Paris Agreement, but exceeding this limit is now assessed as unavoidable under current policies and alternative near-term emissions trajectories [1]. A temperature overshoot occurs when global warming temporarily rises above a specified threshold before returning below it. The consequences of overshoot depend on peak warming, the duration of exceedance and the rate of subsequent cooling, including whether affected systems might cross tipping points or recover as warming declines [1, 2]. However, these consequences remain poorly constrained for ice sheets, whose slow response can sustain impacts for centuries or millennia after atmospheric temperatures decline.

Antarctic recovery depends strongly on ocean conditions. Overshoot simulations show that ocean warming can persist after global surface temperatures decline because the ocean interior adjusts slowly [3, 4, 5]. Continued ocean-driven ice losses are therefore expected even during atmospheric cooling [6, 7]. Ocean-driven melting beneath ice shelves can weaken buttressing, enhance grounding-line retreat, and increase grounded-ice discharge. Ocean adjustment, ice-sheet inertia and hysteresis can prolong sea-level contributions for centuries after atmospheric temperatures decline [5, 7, 8, 9], making end-of-century temperature or sea-level change incomplete measures of Antarctic risk. The question is therefore whether climate recovery following an overshoot can halt further loss, and how the timing of atmospheric and ocean recovery affects the outcome.

Marine-based Antarctic sectors are particularly vulnerable because retrograde bed topography and ice-shelf feedbacks can trigger self-sustaining grounding-line retreat [8, 10, 11], with responses varying among drainage basins [12]. For Greenland, cooling after overshoot can limit long-term ice loss, but idealised simulations still produce peak sea-level contributions of about 0.5 m under rapid recovery and several metres under slower cooling [13]. Most published Antarctic projections examine prescribed emissions pathways through 2100 or 2300, revealing substantial differences among forcing pathways, models

and sectors [14, 15, 16, 17, 18]. Recent coupled Earth system–ice-sheet simulations have explored Antarctic responses to climate overshoot and reversal, highlighting that surface mass balance (SMB), basal melting and ice dynamics complicate the relationship between global temperature and Antarctic mass change [19]. However, how overshoot duration and delayed ocean recovery separately shape Antarctica's additional sea-level contribution remains poorly constrained.

Here we quantify how overshoot duration, represented by the prescribed duration of high climate forcing, and the relative recovery times of atmospheric and ocean forcing shape Antarctica's sea-level contribution through 2300. Using a continental-scale Antarctic ice-sheet model developed for the Ice Sheet Model Intercomparison Project for CMIP7 (ISMIP7), we simulate ice-sheet evolution from a common 2015 initial state under CESM2-WACCM climate forcing. LOW follows an SSP1-2.6-derived low-forcing pathway, whereas HIGH uses SSP3-7.0-derived forcing. Four idealised overshoot experiments apply HIGH for 20, 50, 75 or 100 years before a 10-year transition to LOW (HIGH20, HIGH50, HIGH75 and HIGH100; Fig. 1; Table 1). These prescribed high-forcing intervals represent a proxy for overshoot duration, not the time global temperature exceeds 1.5°C. Further experiments vary forcing magnitude, atmospheric and ocean recovery timing, climate forcing and ice-sheet model physics. We define Antarctic sea-level contribution (ASC) as the cumulative contribution to global mean sea level since 2015, and ΔASC as its difference from the corresponding LOW simulation.

Longer climate overshoot increases Antarctica's additional sea-level contribution

We first quantify how the duration of HIGH forcing during the overshoot experiments affects Antarctica's additional sea-level contribution relative to LOW by 2300. Under LOW, the cumulative ASC reaches 222.9 mm SLE by 2300 and continues to increase at the end of the simulation (Fig. 2a). Relative to LOW, the additional contribution, ΔASC, increases with the duration of high forcing, reaching 1.7, 2.3, 8.6 and 21.5 mm SLE under HIGH20, HIGH50, HIGH75 and HIGH100, respectively (Fig. 2b). The increase from HIGH75 to HIGH100 (12.9 mm) is nearly twice that from HIGH20 to HIGH75 (6.9 mm), hence there is a nonlinear response to the high-forcing duration (Fig. 2c). These overshoot scenarios produce much smaller additional contributions than sustained HIGH forcing, under which ΔASC reaches 65.2 mm SLE by 2300. Recovery towards LOW is slower under HIGH75 and HIGH100: ΔASC peaks at 12.7 mm SLE in 2215 and 27.2 mm SLE in 2252, respectively, before declining to 8.6 and 21.5 mm SLE by 2300 (Fig. 2b).

The duration of HIGH forcing affects the additional sea-level contributions of the three main ice-sheet sectors by 2300 (Fig. 2d). Under HIGH20 and HIGH50, the additional contribution at 2300 is dominated by East Antarctica but remains modest, at 1.8 and 2.2 mm SLE, respectively. In both experiments, the East Antarctic contribution peaks early, at approximately 4.0 mm SLE in 2033, and is smaller thereafter (Supplementary Fig. S5). Under HIGH75, the additional contribution peaks at 6.1 mm SLE in East Antarctica in 2194 and 7.1 mm SLE in West Antarctica in 2215, before declining to 5.1 and 3.8 mm SLE, respectively, by 2300 (Supplementary Fig. S5). East Antarctica therefore remains the larger contributor at 2300, despite the increased West Antarctic response (Fig. 2d). Under HIGH100, West Antarctica becomes the dominant source by 2300, contributing an additional 14.0 mm SLE compared with 7.6 mm from East Antarctica. In all four experiments, there is a reduced contribution from the Antarctic Peninsula by 2300 compared to LOW (Supplementary Table S4).

The response to high-forcing duration is spatially heterogeneous, with the largest sensitivity in the Amundsen Sea Embayment (basin G–H) and Weddell Sea (basin J–Jpp) drainage basins (Supplementary Figs. S6 and S7). In basin J–Jpp, ΔASC increases from −1.1 mm SLE under HIGH20 to 17.1 mm SLE under HIGH100. In contrast, ΔASC in basin G–H decreases from +1.0 to −5.0 mm SLE despite having the largest cumulative ASC under HIGH100 (177 mm SLE). The greater cumulative grounded-ice SMB in G–H under HIGH100 than HIGH20, equivalent to ∼5.7 mm SLE, is consistent with enhanced snowfall under warmer atmospheric forcing partly offsetting ocean-driven ice loss. Together, these experiments show that shortening the high-forcing duration limits Antarctica's additional sea-level contribution when atmospheric and ocean forcing recover together.

We next examine the effects of forcing magnitude and persistence (Fig. 2e). We compare SSP3-7.0-derived HIGH and SSP5-8.5-derived EXTREME forcing applied for 100 years before recovery towards LOW, or maintained through 2300 (Fig. 2e). For the same 100-year high-forcing duration, EXTREME100 produces an additional Antarctic sea-level contribution of 48.8 mm SLE by 2300, compared with 21.5 mm SLE under HIGH100. Among the tested pathways, only sustained EXTREME forcing produces an additional contribution exceeding 1 m by 2300, reaching 1.73 m SLE (Fig. 2e). Thus, forcing recovery can largely reduce Antarctica's additional sea-level contribution even after prolonged exposure to stronger forcing.

We then compare the idealised experiments with the CMIP6 SSP5-3.4-over pathway (OVER534; Fig. 1c), a scenario-based overshoot trajectory in which SSP5-8.5 emissions are followed by strong mitigation from around 2040 [20], with the resulting climate forcing evolving more gradually than our prescribed 10-year transition to LOW. By 2300, OVER534 produces an additional contribution of 70.4 mm SLE relative to LOW, compared with 48.8 mm SLE under EXTREME100, 21.5 mm SLE under HIGH100 and 65.2 mm SLE under sustained HIGH (Fig. 2e). OVER534 remains closer to HIGH100 during the early recovery period, but approaches EXTREME100 by around 2250 and exceeds both by 2300 (Fig. 2e). Over 2125–2300, EXTREME100 more closely matches OVER534 than HIGH100, with a lower root-mean-square difference (14.1 versus

23.3 mm SLE; Supplementary Fig. S11b). These comparisons show that the idealised experiments capture aspects of the OVER534 response, although the OVER534 comparison does not isolate the separate effects of high-forcing duration, forcing magnitude and recovery trajectory.

Delayed ocean recovery amplifies ice loss as snowfall compensation weakens

Ocean warming beneath Antarctic ice shelves can persist even after the atmosphere cools. Coupled ice-sheet–ocean simulations show that the Filchner–Ronne cavity can take more than a century to return to a cold state after climate forcing is reversed [21]. Using HIGH50 as a reference, we test how this ocean memory affects Antarctica's post-overshoot sea-level contribution by independently varying atmospheric and ocean-forcing recovery after a common 50-year period of high forcing (Fig. 3; Fig. 1b). When atmospheric forcing begins to recover but ocean forcing remains high for a longer period, ΔASC continues to grow (Fig. 3a). Relative to synchronous recovery (HIGH50; 2.3 mm SLE by 2300), delaying ocean recovery by 20 years (OCEAN-LAG20) increases ΔASC to 12.4 mm SLE, while a 50-year delay (OCEAN-LAG50) increases it to 44.1 mm SLE. Maintaining high ocean forcing throughout the simulation (OCEAN-PERSIST) increases the additional contribution to 159.3 mm SLE (Fig. 3a,e).

The atmospheric and ocean forcing have opposing effects on the net sea-level response. When atmospheric forcing remains high but ocean forcing recovers without lag (ATM-PERSIST), ΔASC reaches −95.3 mm SLE by 2300 (Fig. 3a,d). In contrast, OCEAN-PERSIST produces positive contributions of 96 and 58 mm SLE from West and East Antarctica, respectively (Fig. 3d), and a larger whole-Antarctic contribution than sustained HIGH (159 versus 65 mm SLE relative to LOW) despite both retaining high ocean forcing. Atmospheric recovery in OCEAN-PERSIST reduces grounded-ice SMB and weakens the snowfall compensation that offsets ocean-driven ice loss under sustained HIGH (Supplementary Fig. S12).

To test whether this atmospheric compensation also matters when ocean forcing eventually recovers, we compare OCEAN-LAG50 with HIGH100. Both prescribe 100 years of high ocean forcing, but atmospheric forcing begins to recover after 50 years in OCEAN-LAG50 and after 100 years in HIGH100. By 2300, OCEAN-LAG50 produces 22.6 mm SLE more ΔASC than HIGH100 (Fig. 3a,d). Between 2065 and 2300, cumulative grounded-ice SMB is greater under HIGH100 by an amount equivalent to 20.2 mm SLE, consistent with increased snowfall partly compensating for ocean-driven ice loss (Supplementary Fig. S13). These comparisons show that earlier atmospheric recovery can weaken snowfall compensation while elevated ocean forcing continues to drive ice loss.

Regional shifts in the response across drainage basins

Delayed ocean recovery broadens the additional sea-level contribution across Antarctica. Under HIGH50, positive ΔASC is confined to 8 of the 18 drainage basins, increasing to 11 under OCEAN-LAG20, 16 under OCEAN-LAG50 and 17 under OCEAN-PERSIST (Supplementary Fig. S14). Under OCEAN-PERSIST, the five leading basins contribute 127.3 mm SLE, approximately 80% of the whole-Antarctic ΔASC (Fig. 4a): 56.5 mm SLE from J–Jpp, approximately 23.0 mm SLE from both G–H and Jpp–K, 13.9 mm SLE from Cp–D and 10.9 mm SLE from Ep–F.

This shift is particularly clear in basin G–H. Despite being the largest source of cumulative Antarctic sea-level contribution under HIGH100 (Supplementary Fig. S6), its ΔASC at 2300 is negative under HIGH50 (−2.8 mm SLE) and OCEAN-LAG20 (−0.6 mm SLE), but rises to 6.2 mm SLE under OCEAN-LAG50 and 23.0 mm SLE under OCEAN-PERSIST. The corresponding grounding-line-flux anomaly becomes larger and more persistent as ocean recovery is delayed (Fig. 4c). This sign change is consistent with the continental-scale competition: increased snowfall can initially compensate for part of the dynamic loss, but this compensation is overtaken when elevated ocean forcing persists. Although the transition point is unresolved, delayed ocean recovery can reverse a major basin's contribution to Antarctica's additional sea-level contribution.

The timing of the dynamical response also differs among basins (Fig. 4b–f). Under OCEAN-PERSIST, the LOW-relative grounding-line-flux anomaly peaks early in basin J–Jpp (144.8 Gt yr^{-1} around 2107) and basin Jpp–K (43.0 Gt yr^{-1} around 2111). Later peaks occur in basin Ep–F (24.2 Gt yr^{-1} around 2205) and basin G–H (134.7 Gt yr^{-1} around 2267). In basin Cp–D, the anomaly is still increasing at 2300, so its maximum is not resolved within the projection period. OCEAN-LAG50 initially produces responses similar to OCEAN-PERSIST in basins J–Jpp and Jpp–K, but the trajectories diverge after ocean recovery begins in OCEAN-LAG50. These contrasting timings show that post-overshoot dynamical response varies among basins: peak grounding-line-flux anomalies occur within decades of atmospheric recovery in some basins and more than a century later in others.

Sensitivity to climate forcing and ice-sheet model configuration

Among the tested configurations, the choice of climate forcing has a larger effect on HIGH100 than either the sliding relation or basal-melt parameterisation (Fig. 5a,c,d). By 2300, HIGH100 produces an additional Antarctic sea-level contribution

of 21.5 mm SLE under CESM2-WACCM forcing, compared with 1.7 mm SLE under MRI-ESM2-0. Under CESM2-WACCM, ΔASC increases monotonically with high-forcing duration, whereas the MRI-ESM2-0 response is smaller and non-monotonic(Fig. 5a). Relative to LOW, cumulative SMB anomalies under HIGH100 are equivalent to +13.7 and +39.1 mm SLE under CESM2-WACCM and MRI-ESM2-0, respectively, whereas cumulative BMB anomalies are −144.9 and −118.4 mm SLE (Supplementary Fig. S4). MRI-ESM2-0 therefore combines greater snowfall compensation with weaker ocean-driven losses, consistent with its smaller additional Antarctic sea-level contribution. Although extending high forcing from 50 to 100 years increases ΔASC under both climate forcings, the duration response differs between the two climate models.

In contrast, the atmosphere–ocean recovery experiments show the same response ordering of ΔASC at 2300 under both climate forcings (Fig. 5b). OCEAN-PERSIST produces the largest additional contribution, followed by OCEAN-LAG50 and synchronous recovery under HIGH50, while ATM-PERSIST produces a negative contribution relative to the matching LOW simulation. Delaying ocean recovery by 50 years increases LOW-relative ΔASC from 2.3 to 44.1 mm SLE under CESM2-WACCM forcing and from 1.0 to 30.1 mm SLE under MRI-ESM2-0 forcing. OCEAN-PERSIST produces 159.3 and 147.6 mm SLE, respectively. Despite differences in magnitude, delayed ocean recovery amplifies Antarctic sea-level contribution under both climate forcings.

Basal-melt configuration affects both the magnitude of the additional contribution and its dependence on high-forcing duration (Fig. 5c). The tests include the 5th-percentile, median and 95th-percentile calibrations of the melt tuning parameter for both the ISMIP6 and ISMIP7 basal-melt parameterisations. Under the ISMIP7 95th-percentile calibration, HIGH50 produces a smaller Antarctic sea-level contribution than its matching LOW simulation ($\Delta ASC < 0$), primarily because reduced grounded-ice loss in basin G–H (approximately −10 mm SLE relative to LOW) outweighs positive contributions elsewhere (Supplementary Fig. S16). The whole-Antarctic response becomes positive under HIGH75 and HIGH100. Basal-melt calibration therefore changes the magnitude and, for some durations, the sign of the additional contribution.

We also test whether the duration response depends on how basal resistance changes as marine-based ice approaches flotation. In the regularised Coulomb relation, C_{max} sets the upper bound on basal shear stress relative to effective pressure. Varying C_{max} from 0.2 to 0.8 therefore tests sensitivity to the strength of this basal-traction limit, with 0.5 used as the reference configuration; the power-law relation provides a comparison without an explicit Coulomb limit (see Methods). Sensitivity to these sliding relations is smaller than sensitivity to basal-melt configurations (Fig. 5c,d). Across all four sliding relations, ΔASC increases with high-forcing duration, and HIGH100 produces similar contributions of 20.4–22.0 mm SLE by 2300 (Fig. 5d). These comparisons indicate limited sensitivity to the sliding formulation within this ensemble, while climate forcing and basal-melt configuration produce larger differences.

Discussion and Conclusions

Our results show that prolonged high climate forcing can increase Antarctica's additional sea-level contribution, while persistent ocean warming after atmospheric recovery can substantially amplify it. When forcing subsequently returns towards the same low-emissions pathway, the additional sea-level contribution built up during the overshoot can persist for centuries. Under the reference CESM2-WACCM forcing with synchronous atmospheric and ocean recovery, the additional contribution at 2300 increases nonlinearly with high-forcing duration. Beginning the transition from HIGH to LOW after 20 rather than 100 years reduces the additional Antarctic sea-level contribution at 2300 by more than 90%, from 21.5 to 1.7 mm SLE. This comparison highlights the potential long-term sea-level benefit of mitigation that shortens exposure to high climate forcing, complementing assessments that emphasise overshoot duration as a climate-risk factor [1]. Nevertheless, ΔASC peaks before 2300, so endpoint values understate the maximum response.

Forcing magnitude also affects the sea-level legacy of overshoot. Within the tested model configuration, greater forcing magnitude increases the additional sea-level contribution for a fixed high-forcing duration, but recovery towards LOW still substantially limits the response compared with sustained extreme forcing. EXTREME illustrates the consequences of prolonged extreme forcing derived from SSP5-8.5, associated with approximately 4.4 °C of global warming by late century relative to 1850–1900 [2], although its underlying twenty-first-century emissions levels are now assessed as implausible in the CMIP7 ScenarioMIP design [22]. The benefit of forcing recovery is consistent with findings for the Greenland Ice Sheet, where rapid cooling after overshoot can limit long-term ice loss, although substantial sea-level contributions may occur before recovery [13]. However, the controls on recovery differ: Greenland's response is strongly linked to atmospheric warming and surface melt, whereas ocean forcing strongly influences Antarctic ice-shelf stability and grounding-line retreat [9, 23, 24]. This makes subsurface ocean warming particularly important for Antarctic recovery.

The benefit of forcing recovery also depends on its timing across climate components. Atmospheric and ocean forcing need not recover together. Ocean warming can persist after global surface temperatures decline because the ocean interior adjusts slowly [3, 4]. The asynchronous atmospheric and ocean recovery prescribed in our idealised overshoot experiments is therefore physically plausible, or perhaps likely, although the duration of the oceanic delay remains uncertain [6]. Coupled simulations show that Antarctic mass balance does not simply track global temperature during climate reversal [19], and that

the Filchner–Ronne cavity can take more than a century to return to a cold state after it has become warm and forcing is reversed [21]. Our experiments complement these studies by quantifying the sea-level consequences of prescribed differences in atmospheric and ocean recovery timing.

The simulated response reflects both persistent ocean-driven losses and weakening surface accumulation compensation. In our experiments, when atmospheric forcing declines but ocean forcing remains high, enhanced snowfall accumulation diminishes while elevated ice-shelf basal melting can continue to weaken buttressing and sustain ice discharge across the grounding line for longer. Atmospheric recovery therefore reduces the accumulation available to counter ongoing ice loss, helping explain why Antarctic sea-level contribution can continue to grow after atmospheric recovery begins. Continued ice loss during climate recovery is consistent with the slow adjustment of the Southern Ocean and the hysteretic response of the ice sheet [6, 8, 25]. The greater contribution under OCEAN-PERSIST than under sustained HIGH, despite their shared ocean-forcing pathway, illustrates the importance of this accumulation effect. This comparison does not imply that mitigation, including carbon dioxide removal used to reverse overshoot, necessarily increases Antarctic ice loss; it identifies a consequence of atmospheric recovery occurring ahead of ocean recovery.

In our experiments, even a two-decade delay in ocean recovery (OCEAN-LAG20) increases the additional sea-level contribution more than fivefold relative to synchronous recovery (HIGH50), while a 50-year delay further amplifies this response. The post-overshoot response therefore depends on the relative timing of ocean-forcing recovery and the decline in surface accumulation, as well as the ice sheet's dynamic adjustment. Resolving surface mass balance alongside the ocean's memory of climate overshoot is therefore a research priority, particularly how snowfall accumulation evolves relative to the persistence of warm ocean conditions beneath Antarctic ice shelves during atmospheric cooling.

Our basin-scale analysis shows that what looks like a modest Antarctic sea level contribution may conceal substantial regional differences when ocean recovery is delayed. Basin contributions depend on the evolving balance between snowfall accumulation and ocean-driven dynamic ice loss, so their relative importance can change when ocean recovery is delayed. Contrasting response times further imply that an apparent stabilisation in one sector need not indicate Antarctic-wide recovery. Because the regional pattern of sea-level rise depends on where Antarctic mass is lost [16, 26], this evolving distribution could alter regional sea-level fingerprints even for a similar global-mean Antarctic contribution, an effect not quantified here. Basin-scale tipping-risk assessments should therefore consider ocean-forcing persistence and recovery timing [12, 27], although our experiments do not identify tipping thresholds.

The sensitivity experiments show that the balance between surface accumulation and ocean-driven dynamic ice loss shapes the response to high-forcing duration. Under CESM2-WACCM forcing, HIGH100 produces a larger additional sea-level contribution than the shorter-duration experiments across all tested sliding relations and basal-melt parameterisations. Under MRI-ESM2-0, greater surface accumulation and a smaller increase in basal melting relative to LOW are consistent with the smaller additional sea-level contribution, while the response to high-forcing duration is non-monotonic. Despite these differences, delayed ocean recovery produces a more consistent response: both climate forcings yield larger additional contributions when ocean recovery is delayed or prevented. Although differences in accumulation and ocean-driven losses introduce uncertainty into the magnitude and timing of the projected contribution, this agreement supports ocean-recovery timing as a key control on Antarctica's post-overshoot sea-level contribution.

Our idealised experiments isolate how high-forcing duration and atmosphere–ocean recovery timing affect Antarctic sea-level contribution, but do not predict a specific future climate trajectory. Prescribed climate forcing and parameterised ice-shelf basal melting cannot capture the full feedbacks between climate, ocean circulation and ice-sheet evolution, while the absence of evaluation against observed transient mass loss limits confidence in the projected magnitudes. The sensitivity experiments nevertheless allow us to assess which findings persist across the tested model configurations and climate forcings.

Taken together, our results show that limiting the duration of high forcing can reduce Antarctica's additional sea-level contribution, but delayed ocean recovery in the post-overshoot period can substantially reduce this benefit. Rapid atmospheric recovery may further weaken this benefit by reducing snowfall accumulation while persistent high ocean forcing continues to drive dynamic ice loss. Assessing Antarctica's sea-level legacy requires considering both how long high forcing persists and the relative timing of atmospheric and ocean recovery. Further development and evaluation of coupled ice-sheet-ocean models, together with improved climate forcing datasets, will help constrain this timing and its implications for Antarctic ice loss. Our results underscore why this matters: atmospheric recovery is not ice-sheet recovery.

Methods

Ice-sheet model configuration

The simulations use an Antarctic model configuration developed for ISMIP7, but the idealised overshoot experiments are not part of the standard ISMIP7 protocol. Ice dynamics are simulated with the open-source finite-element model Elmer/Ice [28], using the shallow–shelf approximation (SSA) [29] to solve the vertically integrated momentum equations.

The model geometry comes from the MEaSUREs BedMachine Antarctica Version 4 dataset [30, 31], including the upper and lower ice surfaces and bedrock topography. An unstructured finite-element mesh is first generated with Gmsh [32] following the Antarctic coastline defined by BedMachine. The mesh is then refined with MMG [33] according to ice-thickness gradients and the Hessian of observed surface velocity from the MEaSUREs Phase-Based Antarctica Ice Velocity map [34]. The resulting mesh has a horizontal resolution of about 1 km in fast-flowing ice and near the grounding line, coarsening to about 25 km in the interior (Supplementary Fig. S1). Bedrock elevation is held fixed, excluding glacial isostatic adjustment and its effects on water depth and grounding-line stability.

Antarctic projections obtained on this 1 km mesh agree with simulations at 500 m resolution with the same model and grounding-line treatment [35]. All paired forcing experiments use the same mesh and the analysis rests on differences between simulations, so mesh-dependent biases in ASC are reduced, though they may not cancel completely.

Spatial tuning of parameters governing basal resistance and ice viscosity is implemented through adjoint-based inversions that minimise the mismatch between simulated and observed surface velocity (Supplementary Fig. S2). The inversion framework follows Zhao et al. [35], but the sliding relation, inversion sequence, and regularisation parameters were re-evaluated for the present ISMIP7 configuration (Supplementary Methods). Simulations employ either a conventional power-law (Weertman) sliding relation [36], or a regularised Coulomb sliding relation [37, 38].

For the power-law sliding relation we define,

$$\tau_b = \beta^2 |\mathbf{u}_b|^{m-1} \mathbf{u}_b, \tag{1}$$

where τ_b is basal shear stress, $\mathbf{u}_b$ is basal sliding velocity and β^2 is spatially varying basal-friction coefficient inferred by adjoint inversion. The velocity exponent is $m = 1/n = 1/3$, that is, a Weertman exponent $n = 3$.

The regularised Coulomb relation is written as,

$$\tau_b = C_{\max} N \left(\frac{\chi}{1+\chi} \right)^{1/n} \frac{\mathbf{u}_b}{|\mathbf{u}_b|}, \tag{2}$$

where

$$\chi = \frac{|\mathbf{u}_b|}{A_s (C_{\max} N)^n}, \qquad n = 3. \tag{3}$$

Here, A_s is the spatially varying sliding parameter inferred by adjoint inversion, related to the power-law friction coefficient by $\beta^2 = A_s^{-m}$. N is effective pressure, and $C_{\max}$ specifies the upper bound on the ratio of basal shear stress to effective pressure. We set the post-peak exponent to $q = 1$, as incorporated in the equation above, so that basal drag approaches the Coulomb limit $C_{\max} N$ asymptotically without velocity weakening at fixed effective pressure. Effective pressure is calculated using the perfect-ocean-connection approximation,

$$N_{\mathrm{POC}} = \rho_i g H + \rho_o g z_b, \tag{4}$$

where H is ice thickness, z_b is bed elevation relative to sea level (positive upwards), and $\rho_i = 917\ \mathrm{kg\,m^{-3}}$ and $\rho_o = 1028\ \mathrm{kg\,m^{-3}}$ are the densities of ice and ocean water. Effective pressure falls as grounded marine ice approaches flotation. For numerical stability, the effective pressure in the sliding relation is bounded below $N_{\min} = 0.05$ MPa. Because the area over which this bound is active was not quantified, the lower bound may also influence basal resistance in regions of low effective pressure. Effective pressure does not evolve through a subglacial hydrology model, so hydrological feedbacks on basal resistance are not represented [35].

The sliding relation tends to power-law sliding when $\chi \ll 1$ and to Coulomb-limited sliding when $\chi \gg 1$. $C_{\max}$ therefore controls the upper limit on basal traction relative to effective pressure and the area over which basal motion is Coulomb limited [39]. $C_{\max}$ is an effective coefficient for the Coulomb-limited basal strength and represents unresolved properties of the ice–bed interface. We adopt $C_{\max} = 0.5$ as the reference configuration because this value gives a moderate Coulomb limitation. In our model, $C_{\max} = 0.8$ behaves close to the calibrated power-law solution, and $C_{\max} = 0.2$ represents a substantially stronger Coulomb-limited end member. Sensitivity to the choice of $C_{\max}$ is assessed with $C_{\max} = 0.8$ and 0.2 and the power-law configuration (Supplementary Table S1). The meaning of the transition between the two regimes for Antarctic ice dynamics is discussed by Zhao et al. [35].

Grounding-line migration uses the sub-element parameterisation with 20 integration points per element [40, 41]. The ice front is held fixed; calving-front migration and ice-shelf collapse are not explicitly represented. Ice-shelf collapse could accelerate grounding-line retreat and discharge in some sectors [27]. Because it could affect both LOW and the overshoot experiments, its omission does not establish a lower bound on ΔASC. Ice-shelf basal melting uses the SEM3 treatment, in

which melt is applied over the floating fraction of partially grounded elements, and melt at the grounding line is evaluated with the same 20-point integration, an approach acceptable at 1 km resolution [41].

Ice-shelf basal melt in the reference configuration is calculated from the time-varying ocean thermal forcing with the ISMIP7 local-quadratic parameterisation [42]. The parameterisation depends on far-field thermal forcing, temperature and salinity, extrapolated to the local ice shelf draft, the Coriolis parameter and the ice-draft slope. We prescribe a constant ice draft slope, $\sin(\theta) = 9.80 \times 10^{-3}$, calculated as the floating-area-weighted Antarctic mean from the BedMachine Antarctica ice-shelf geometry [30] on the 1 km model mesh.

The dimensionless melt tuning parameter K was calibrated for this model configuration with fixed present-day geometry and seven observational and model-derived ocean states, following the ISMIP7 basal-melt calibration framework [42]. Melt was diagnosed on the native unstructured mesh, including the effective SEM3 treatment, and conservatively remapped to the 2-km ISMIP evaluation grid. The calibration procedure optimises melt rate (and thus K) against satellite observations, climatologies and modelled cold and warm ocean forcing, and melt rate observations. The 5th-percentile, median and 95th-percentile values of the fitted distribution are $K_{05} = 2.50 \times 10^{-5}$, $K_{50} = 4.75 \times 10^{-5}$ and $K_{95} = 7.75 \times 10^{-5}$.

The reference configuration uses K_{50} with basin-specific thermal-forcing offsets, ΔT_b, which correct regional biases in present-day basal melting not captured by a single Antarctic-wide K. The offsets are added to the ocean thermal forcing in each basin. Sensitivity to the basal-melt magnitude is assessed with the K_{05} and K_{95} configurations and the same offsets.

We assess structural and parametric uncertainty with the ISMIP6 local-quadratic basal-melt formulation [43]. These experiments use the published 5th-percentile, median and 95th-percentile calibration of the local MeanAnt calibration, $\gamma_{0,05} = 7710$, $\gamma_{0,50} = 11075.45$ and $\gamma_{0,95} = 15300$ m yr^{-1}. As in the ISMIP6 protocol, basin-dependent thermal-forcing corrections (δT_{sector}) reproduce present-day sector melt rates and correct for unresolved cavity processes and observational biases. Both parameterisations use extrapolated ocean thermal forcing that evolves with the climate forcing. But neither resolves circulation within ice-shelf cavities [44, 45, 46] or the influence of subglacial discharge on basal melting [47, 48].

Initialisation and climate forcing

The inverted basal-friction and ice-viscosity fields and the initial geometry, form the initial state for all simulations. This state represents observations from about 2005 and is run through a historical simulation (2005–2014) with historical climate forcing so that the model can adjust. The 2015 state is the common initial condition for all projection experiments from 2015 to 2300. Atmospheric and ocean forcing for the projection come from the CESM2-WACCM climate model following the ISMIP7 protocol [49]. Although initial model parameters are constrained by observed surface velocity, the simulated transient mass loss has not been evaluated against observations.

SMB is prescribed from the downscaled monthly ISMIP7 SMB forcing and corrected for changes in ice-surface elevation relative to the reference topography of the downscaling, following the ISMIP6 Greenland protocol [50], with the same formula applied here to Antarctica:

$$\mathrm{SMB}(x,y,t) = \mathrm{acabf}(x,y,t) + \frac{\partial \mathrm{SMB}}{\partial z}(x,y,t)\,[z_s(x,y,t) - z_{s,\mathrm{ref}}(x,y)]\,, \tag{5}$$

where acabf is the downscaled monthly SMB, $\partial \mathrm{SMB}/\partial z$ is the prescribed SMB–elevation gradient, z_s is the modelled ice-surface elevation and $z_{s,\mathrm{ref}}$ is the reference surface of the ISMIP7 downscaling. We use the Reference Elevation Model of Antarctica data used in the ISMIP7 SMB downscaling as $z_{s,\mathrm{ref}}$. The integrated SMB in Elmer/Ice (2574 Gt yr^{-1} in 2005) agrees to approximately 2.5% with the ISMIP7 CESM2-WACCM historical climatology (2511 Gt yr^{-1}), indicating that the forcing was read and converted correctly.

The forcing fields modified during preprocessing are ocean thermal forcing (`tf`), practical salinity (`so`) and the SMB fields `acabf` and `dacabfdz`. All other forcing variables are unchanged from the ISMIP7 datasets(Supplementary Table S3).

Because SSP3-7.0 forcing is unavailable beyond 2100, and SSP1-2.6 extends to 2300, we construct the post-2100 HIGH forcing by adding a late-century SSP3-7.0–SSP1-2.6 climatological anomaly to the evolving SSP1-2.6 forcing. For each calendar month m, we calculate the mean scenario anomaly over 2081–2100,

$$\Delta F_m(x,y) = \Big\langle F_{\mathrm{SSP3-7.0}}(m,x,y) - F_{\mathrm{SSP1-2.6}}(m,x,y) \Big\rangle_{2081\text{–}2100}, \tag{6}$$

and construct the extended high-forcing field as

$$F_{\mathrm{HIGH}}(t,x,y) = F_{\mathrm{SSP1-2.6}}(t,x,y) + \Delta F_{m(t)}(x,y), \qquad t > 2100, \tag{7}$$

where $m(t)$ is the calendar month at time t, and $\langle\cdot\rangle_{2081\text{–}2100}$ is the mean over 2081–2100. The construction keeps the evolving SSP1-2.6 background and its interannual variability and keeps the mean seasonal and spatial contrast between SSP3-7.0 and

SSP1-2.6 of the late twenty-first century. No repeated multi-year SSP3-7.0 sequence is needed beyond 2100. The extension is a continuation of the late-century SSP3-7.0–SSP1-2.6 contrast, not a climate-model projection of SSP3-7.0 beyond 2100.

The procedure is applied to all four forcing fields: ocean thermal forcing (`tf`), practical salinity (`so`), surface mass balance (`acabf`), and the SMB–elevation gradient (`dacabfdz`). For `tf` and `dacabfdz`, whose anomalies were still evolving near 2100, the late-century anomaly is blended linearly into the 2081–2100 climatological anomaly over 2101–2110 and held fixed thereafter. For `acabf` and `so`, the climatological anomaly is applied directly after 2100 without an additional transition. Experiments with persistent HIGH atmospheric or ocean forcing retain the corresponding extended HIGH forcing components through 2300.

Experiment design

Unless stated otherwise, the primary suite uses the RC05 regularised Coulomb sliding configuration ($C_{\max} = 0.5$) and the median calibrated ISMIP7 local quadratic basal-melt configuration (K_{50}) with basin-specific thermal-forcing offsets.

The low-forcing reference experiment (LOW) follows the SSP1-2.6 pathway, and the sustained high-forcing experiment (HIGH) follows SSP3-7.0. These scenarios provide contrasting forcing trajectories within the available CMIP6-based ISMIP7 datasets. SSP1-2.6 provides a lower-forcing reference and recovery pathway, while SSP3-7.0 provides the higher-forcing trajectory whose duration is varied across the primary experiments. We assess sensitivity to stronger forcing using sustained extreme-forcing experiment (EXTREME) driven by SSP5-8.5. We also construct EXTREME100, in which SSP5-8.5 forcing is kept for 100 years before returning towards the LOW pathway, which separates the effects of forcing magnitude and persistence. We also include the CMIP6 SSP5-3.4-over pathway (OVER534) as a scenario-based overshoot benchmark with a transient overshoot and a decline; it is not used in the construction of the idealised experiments.

The controlled high-forcing experiments combine the preprocessed SSP3-7.0 and SSP1-2.6 forcing fields through a prescribed time-dependent transition not through further climate-model simulations. High-forcing duration is the prescribed length of the SSP3-7.0-derived forcing phase from the start of the projection in 2015, rather than the number of years above a global-mean temperature threshold.

Atmospheric and ocean forcing initially follow HIGH, then transition towards LOW over 10 years. Thereafter, forcing follows the LOW pathway to 2300. HIGH20, HIGH50, HIGH75 and HIGH100 prescribe 20, 50, 75 and 100 years of SSP3-7.0-derived high forcing, respectively, before the transition begins. Longer HIGH periods increase both the duration of high forcing and cumulative forcing exposure; the experiments therefore do not isolate their separate effects. HIGH50 serves as the control for the atmosphereocean recovery experiments.

For each forcing component, the transition is prescribed as

$$F(t) = w(t)F_{\mathrm{HIGH}}(t) + [1 - w(t)]F_{\mathrm{LOW}}(t), \tag{8}$$

where F_{HIGH} and F_{LOW} are the HIGH and LOW forcing fields and $w(t)$ is a weight. During the high-forcing phase $w = 1$; w then falls linearly to zero over the 10-year transition and stays zero after. The same timing applies to the atmospheric(SMB) and ocean components in the duration experiments.

A second group of experiments isolates the effects of asynchronous atmospheric and ocean recovery. These experiments start from HIGH50, in which atmospheric and ocean forcing recover together after 50 years of HIGH forcing. The recovery of one component is changed and the 50-year high-forcing period is kept.

In ATM-PERSIST, atmospheric forcing remains on the HIGH pathway while ocean forcing recovers to LOW. In OCEAN-LAG20 and OCEAN-LAG50, atmospheric forcing recovers after 50 years, and ocean recovery is delayed by a further 20 and 50 years. In OCEAN-PERSIST, atmospheric forcing recovers after 50 years while ocean forcing remains on the HIGH pathway to 2300. These experiments separate the effects of finite ocean-recovery delay from those of persistent high ocean forcing.

The primary and recovery experiments are listed in Table 1.

To assess whether Antarctica's sea-level contribution depends on the main modelling choices, we evaluate three sources of uncertainty (Supplementary Table S1). Basal-sliding sensitivity is assessed with the power-law configuration and the regularised Coulomb configurations RC08 ($C_{\max} = 0.8$), RC05 ($C_{\max} = 0.5$) and RC02 ($C_{\max} = 0.2$), with RC05 as the reference.

Ice-shelf basal-melt uncertainty is assessed with the calibrated 5th-percentile, median and 95th-percentile parameter sets of the ISMIP7 local quadratic formulation and the ISMIP6 local quadratic formulation as a structural sensitivity. Climate-forcing sensitivity is assessed by repeating LOW, HIGH20, HIGH50, HIGH75, HIGH100, ATM-PERSIST, OCEAN-LAG50 and OCEAN-PERSIST with MRI-ESM2-0 forcing, alongside the reference CESM2-WACCM forcing. For each configuration, each experiment is compared with the matching LOW simulation to remove differences in background evolution.

Diagnostics and sea-level contribution

The ice-sheet response is quantified by Antarctica's sea-level contribution, basin mass change, and ice flux across the grounding line, ice-shelf basal melt and grounded area. The contribution is calculated from the change in grounded ice volume above

Table 1. Primary experiments for Antarctica's sea-level contribution under climate overshoot. The forcing pathways are drawn in Fig. 1.

Experiment	Atmospheric(SMB) forcing	Ocean forcing
Reference simulations		
LOW	SSP1-2.6	SSP1-2.6
HIGH	SSP3-7.0	SSP3-7.0
Controlled high forcing		
HIGH20	SSP3-7.0 for 20 yr, then SSP1-2.6	SSP3-7.0 for 20 yr, then SSP1-2.6
HIGH50	SSP3-7.0 for 50 yr, then SSP1-2.6	SSP3-7.0 for 50 yr, then SSP1-2.6
HIGH75	SSP3-7.0 for 75 yr, then SSP1-2.6	SSP3-7.0 for 75 yr, then SSP1-2.6
HIGH100	SSP3-7.0 for 100 yr, then SSP1-2.6	SSP3-7.0 for 100 yr, then SSP1-2.6
Atmosphere–ocean recovery experiments		
ATM-PERSIST	SSP3-7.0 throughout	SSP3-7.0 for 50 yr, then SSP1-2.6
OCEAN-LAG20	SSP3-7.0 for 50 yr, then SSP1-2.6	SSP3-7.0 for 70 yr, then SSP1-2.6
OCEAN-LAG50	SSP3-7.0 for 50 yr, then SSP1-2.6	SSP3-7.0 for 100 yr, then SSP1-2.6
OCEAN-PERSIST	SSP3-7.0 for 50 yr, then SSP1-2.6	SSP3-7.0 throughout
Forcing magnitude and persistence		
EXTREME100	SSP5-8.5 for 100 yr, then SSP1-2.6	SSP5-8.5 for 100 yr, then SSP1-2.6
EXTREME	SSP5-8.5 throughout	SSP5-8.5 throughout
Scenario-based overshoot benchmark		
OVER534	SSP5-3.4-over	SSP5-3.4-over

LOW, HIGH and EXTREME denote forcing derived from SSP1-2.6, SSP3-7.0 and SSP5-8.5. For HIGH20–HIGH100 and EXTREME100, the appended number is the duration of high forcing before recovery begins. Recovery is prescribed as a 10-yr transition towards the LOW pathway. OVER534 is the SSP5-3.4-over CMIP6 overshoot experiment. Unless stated otherwise, primary experiments use the RC05 sliding-relation configuration and the calibrated reference ice-shelf basal-melt parameterisation. Sensitivity experiments are listed in Supplementary Table S1.

flotation since 2015; positive values are a rise in global mean sea level. Basin and regional contributions are calculated using the fixed mask of 18 drainage basins from the Ice Sheet Mass Balance Inter-comparison Exercise (IMBIE; Supplementary Methods) [51], and their sum defines the reported whole-Antarctic contribution. The conversion to sea-level equivalent uses an ocean area of $3.625 \times 10^{14}\,\mathrm{m}^2$(Supplementary Methods). We define Antarctica's sea-level contribution as ASC. This is the contribution simulated up to time t under a prescribed forcing pathway; it does not represent equilibrium or irreversible ice loss.

To isolate the additional effect from high forcing, we calculate the difference from the matching low-forcing simulation:

$$\Delta\mathrm{ASC}_{e,c}(t) = \mathrm{ASC}_{e,c}(t) - \mathrm{ASC}_{\mathrm{LOW},c}(t), \tag{9}$$

where e denotes the forcing experiment and c the model configuration. The LOW simulation uses the corresponding climate-model forcing and model-physics choices. A positive ΔASC means a greater sea-level contribution than LOW; a negative value means a smaller contribution, not necessarily ice gain.

For the climate-model comparison, SMB and BMB anomalies relative to the matching LOW simulation are spatially integrated over the full model domain, including grounded and floating ice, and accumulated over 2015–2300. These cumulative anomalies are expressed as mass equivalents in mm SLE, rather than direct sea-level contributions. In particular, ice-shelf basal melting affects sea level through its influence on grounded-ice dynamics.

To compare the idealised experiments with OVER534, we calculate the root-mean-square difference (RMSD) between the annual LOW-relative contribution trajectories over 2125–2300 (Supplementary Methods). The idealised trajectories are linearly interpolated to the OVER534 output years where necessary. RMSD is calculated from unsmoothed annual values with equal weighting across years; a smaller value means closer agreement in timing and magnitude.

Data availability

Original ISMIP7 forcing datasets from several climate models are available from the ISMIP7 webpage (https://www.ismip.org/research/ismip7). The MEaSUREs BedMachine Antarctica, Version 4 is available at https://nsidc.

org/data/nsidc-0756/versions/4. The MEaSUREs Phase-Based Antarctica Ice Velocity map (Version 1) is available at https://nsidc.org/data/nsidc-0754/versions/1. Processed source data supporting the main and supplementary figures and the unpartitioned Antarctic computational mesh are archived on Zenodo at https://doi.org/10.5281/zenodo.23213185. Study-specific forcing and restart files are too large to include in the archive and are available from the corresponding author upon reasonable request.

Code availability

Elmer/Ice is available from the ElmerFEM GitHub repository (https://github.com/ElmerCSC/elmerfem) with latest releases from https://doi.org/10.5281/zenodo.19888172. Representative Elmer/Ice configurations, supporting Lua files, and Fortran source files are archived on Zenodo at https://doi.org/10.5281/zenodo.23213185. Configurations for other experiments and ensemble members, and additional supporting files are available from the corresponding author upon reasonable request.

Acknowledgements

C.Z. is the recipient of an Australian Research Council (ARC) Discovery Early Career Researcher Award (project number DE240100267) funded by the Australian Government. C.Z., M.A.K., and P.C. are supported by the ARC Special Research Initiative, Australian Centre for Excellence in Antarctic Science (project number SR200100008). C.Z., D.G., B.G received grant funding from the Australian Government as part of the Antarctic Science Collaboration Initiative program (ASCI000002). R.G. is supported by the Research Council of Finland grant number 355572. T.Z. is supported by the Research Council of Finland grant number 322978. E.J. is supported by the Research Council of Finland grant number 355783. M.A.K is supported by an ARC Laureate Fellowship (FL250100022). We thank CSC – IT Center for Science Ltd (Finland) for allocating computational resources on LUMI. LUMI is owned by the EuroHPC Joint Undertaking and hosted in Finland by CSC together with the LUMI consortium. This work is also supported by resources provided by the Pawsey Supercomputing Research Centre's Setonix Supercomputer (https://doi.org/10.48569/18sb-8s43), with funding from the Australian Government and the Government of Western Australia. We thank the ISMIP7 steering committee and focus groups for their continued efforts in developing ISMIP7 and providing its protocols and forcing datasets.

Author contributions

C.Z. conceived and led the study, designed the experiments, performed the simulations, analysed the results, prepared the figures, and wrote the first draft of the manuscript. R.G., T.Z. and E.J. contributed to ice-sheet model development. D.G. contributed to the basal-melt calibration framework and interpretation of the results. All authors contributed to the development of the study, discussed the results, edited the manuscript, and approved the final version.

Competing interests

The authors declare no competing interests.

References

1. United Nations Environment Programme. Limiting Overshoot: Navigating exceedance of 1.5°C and pathways towards return. Tech. Rep., United Nations Environment Programme (2026). DOI: 10.59117/20.500.11822/49857.

2. IPCC. Climate Change 2023: Synthesis Report. Contribution of Working Groups I, II and III to the Sixth Assessment Report of the Intergovernmental Panel on Climate Change, DOI: 10.59327/ipcc/ar6-9789291691647 (2023).

3. Schwinger, J., Asaadi, A., Steinert, N. J. & Lee, H. Emit now, mitigate later? Earth system reversibility under overshoots of different magnitudes and durations. *Earth Syst. Dyn.* **13**, 1641–1665, DOI: 10.5194/esd-13-1641-2022 (2022).

4. Schleussner, C. F. *et al.* Overconfidence in climate overshoot. *Nature* **634**, 366–373, DOI: 10.1038/s41586-024-08020-9 (2024).

5. Stokes, C. R., Bamber, J. L., Dutton, A. & DeConto, R. M. Warming of +1.5°C is too high for polar ice sheets. *Commun. Earth & Environ.* **6**, 351, DOI: 10.1038/s43247-025-02299-w (2025).

6. Fox-Kemper, B. *et al.* Ocean, Cryosphere and Sea Level Change. In Masson-Delmotte, V. *et al.* (eds.) *Climate Change 2021: The Physical Science Basis. Contribution of Working Group I to the Sixth Assessment Report of the Intergovernmental Panel on Climate Change*, chap. 9, 1211–1361, DOI: 10.1017/9781009157896.011 (Cambridge University Press, Cambridge, UK and New York, NY, USA, 2021).

7. Stokes, C. R. *et al.* Response of the East Antarctic Ice Sheet to past and future climate change. *Nature* **608**, 275–286, DOI: 10.1038/s41586-022-04946-0 (2022).

8. Garbe, J., Albrecht, T., Levermann, A., Donges, J. F. & Winkelmann, R. The hysteresis of the Antarctic Ice Sheet. *Nature* **585**, 538–544, DOI: 10.1038/s41586-020-2727-5 (2020).

9. Naughten, K. A., Holland, P. R. & De Rydt, J. Unavoidable future increase in West Antarctic ice-shelf melting over the twenty-first century. *Nat. Clim. Chang.* **13**, 1222–1228, DOI: 10.1038/s41558-023-01818-x (2023).

10. Schoof, C. Ice sheet grounding line dynamics: Steady states, stability, and hysteresis. *J. Geophys. Res. Earth Surf.* **112**, DOI: 10.1029/2006jf000664 (2007).

11. Pattyn, F. *et al.* The Greenland and Antarctic ice sheets under 1.5 °C global warming. *Nat. Clim. Chang.* **8**, 1053–1061, DOI: 10.1038/s41558-018-0305-8 (2018).

12. Winkelmann, R., Garbe, J., Donges, J. F. & Albrecht, T. Mapping tipping risks from Antarctic ice basins under global warming. *Nat. Clim. Chang.* **16**, 341–349, DOI: 10.1038/s41558-025-02554-0 (2026).

13. Bochow, N. *et al.* Overshooting the critical threshold for the Greenland ice sheet. *Nature* **622**, 528–536, DOI: 10.1038/s41586-023-06503-9 (2023).

14. Seroussi, H. *et al.* ISMIP6 Antarctica: a multi-model ensemble of the Antarctic ice sheet evolution over the 21st century. *The Cryosphere* **14**, 3033–3070, DOI: 10.5194/tc-14-3033-2020 (2020).

15. Edwards, T. L. *et al.* Projected land ice contributions to twenty-first-century sea level rise. *Nature* **593**, 74–82, DOI: 10.1038/s41586-021-03302-y (2021).

16. Lin, Y. *et al.* Committed Antarctic Ice Sheet mass loss by the end of the twenty-first century. *Nat. Geosci.* DOI: 10.1038/s41561-026-02102-1 (2026).

17. Seroussi, H. *et al.* Evolution of the Antarctic Ice Sheet Over the Next Three Centuries From an ISMIP6 Model Ensemble. *Earth's Futur.* **12**, e2024EF004561, DOI: 10.1029/2024ef004561 (2024).

18. Coulon, V. *et al.* From short-term uncertainties to long-term certainties in the future evolution of the Antarctic Ice Sheet. *Nat. Commun.* **16**, 10385, DOI: 10.1038/s41467-025-66178-w (2025).

19. Smith, R. S. *et al.* Response of ice sheets, sea-ice and sea level in climate stabilisation and reversibility simulations using a state-of-the-art Earth System Model. *Earth Syst. Dyn.* **17**, 475–493, DOI: 10.5194/esd-17-475-2026 (2026).

20. O'Neill, B. C. *et al.* The Scenario Model Intercomparison Project (ScenarioMIP) for CMIP6. *Geosci. Model. Dev.* **9**, 3461–3482, DOI: 10.5194/gmd-9-3461-2016 (2016).

21. Reese, R., De Rydt, J. & Naughten, K. A. Ice-SheetOcean Interactions and the Reversibility of a Regime Shift Beneath Filchner-Ronne Ice Shelf. *J. Geophys. Res. Ocean.* **131**, e2025JC023952, DOI: 10.1029/2025jc023952 (2026).

22. Van Vuuren, D. P. *et al.* The Scenario Model Intercomparison Project for CMIP7 (ScenarioMIP-CMIP7). *Geosci. Model. Dev.* **19**, 2627–2656, DOI: 10.5194/gmd-19-2627-2026 (2026).

23. Rosevear, M. G., Gayen, B., Vreugdenhil, C. A. & Galton-Fenzi, B. K. How Does the Ocean Melt Antarctic Ice Shelves? *Annu. Rev. Mar. Sci.* **17**, 325–353, DOI: 10.1146/annurev-marine-040323-074354 (2025).

24. Adusumilli, S., Fricker, H. A., Medley, B., Padman, L. & Siegfried, M. R. Interannual variations in meltwater input to the Southern Ocean from Antarctic ice shelves. *Nat. Geosci.* **13**, 616–620, DOI: 10.1038/s41561-020-0616-z (2020).

25. McCormack, F. S. *et al.* The Impact of Variable Ocean Temperatures on Totten Glacier Stability and Discharge. *Geophys. Res. Lett.* **48**, e2020GL091790, DOI: 10.1029/2020gl091790 (2021).

26. Zhao, C. *et al.* Antarctic sea-level fingerprints amplify future sea-level rise across Pacific Islands. ESS Open Archive preprint, DOI: 10.22541/essoar.15009379/v1 (2026).

27. Fricker, H. A. *et al.* Antarctica in 2025: Drivers of deep uncertainty in projected ice loss. *Science* **387**, 601–609, DOI: 10.1126/science.adt9619 (2025).

28. Gagliardini, O. *et al.* Capabilities and performance of Elmer/Ice, a new-generation ice sheet model. *Geosci. Model. Dev.* **6**, 1299–1318, DOI: 10.5194/gmd-6-1299-2013 (2013).

29. MacAyeal, D. R. Large-scale ice flow over a viscous basal sediment: Theory and application to ice stream B, Antarctica. *J. Geophys. Res. Solid Earth* **94**, 4071–4087, DOI: 10.1029/jb094ib04p04071 (1989).

30. Morlighem, M. *et al.* Deep glacial troughs and stabilizing ridges unveiled beneath the margins of the Antarctic ice sheet. *Nat. Geosci.* **13**, 132–137, DOI: 10.1038/s41561-019-0510-8 (2020).

31. Morlighem, M. MEaSUREs BedMachine Antarctica, Version 4, DOI: 10.5067/pojqi54a45hx (2025).

32. Geuzaine, C. & Remacle, J.-F. Gmsh: A 3-D finite element mesh generator with built-in pre- and post-processing facilities. *Int. J. for Numer. Methods Eng.* **79**, 1309–1331, DOI: 10.1002/nme.2579 (2009).

33. Dobrzynski, C. & Frey, P. Anisotropic Delaunay Mesh Adaptation for Unsteady Simulations. In Garimella, R. V. (ed.) *Proceedings of the 17th International Meshing Roundtable*, 177–194, DOI: 10.1007/978-3-540-87921-3_11 (Springer Berlin Heidelberg, Berlin, Heidelberg, 2008).

34. Mouginot, J., Rignot, E. & Scheuchl, B. Continent-Wide, Interferometric SAR Phase, Mapping of Antarctic Ice Velocity. *Geophys. Res. Lett.* **46**, 9710–9718, DOI: 10.1029/2019gl083826 (2019).

35. Zhao, C. *et al.* Subglacial water amplifies Antarctic contributions to sea-level rise. *Nat. Commun.* **16**, 3187, DOI: 10.1038/s41467-025-58375-4 (2025).

36. Weertman, J. On the Sliding of Glaciers. *J. Glaciol.* **3**, 33–38, DOI: 10.3189/s0022143000024709 (1957).

37. Schoof, C. The effect of cavitation on glacier sliding. *Proc. Royal Soc. A: Math. Phys. Eng. Sci.* **461**, 609–627, DOI: 10.1098/rspa.2004.1350 (2005).

38. Gagliardini, O., Cohen, D., Råback, P. & Zwinger, T. Finite-element modeling of subglacial cavities and related friction law. *J. Geophys. Res. Earth Surf.* **112**, DOI: 10.1029/2006jf000576 (2007).

39. Joughin, I., Smith, B. E. & Schoof, C. G. Regularized Coulomb Friction Laws for Ice Sheet Sliding: Application to Pine Island Glacier, Antarctica. *Geophys. Res. Lett.* **46**, 4764–4771, DOI: 10.1029/2019gl082526 (2019).

40. Seroussi, H., Morlighem, M., Larour, E., Rignot, E. & Khazendar, A. Hydrostatic grounding line parameterization in ice sheet models. *The Cryosphere* **8**, 2075–2087, DOI: 10.5194/tc-8-2075-2014 (2014).

41. Wang, Y. *et al.* Sensitivity of the future evolution of the Wilkes Subglacial Basin ice sheet to grounding-line melt parameterizations. *The Cryosphere* **18**, 5117–5137, DOI: 10.5194/tc-18-5117-2024 (2024).

42. Reese, R. *et al.* A protocol for calibrating basal melt rates in the ISMIP7 Antarctic ice sheet projections. *EGUsphere* 1–56, DOI: 10.5194/egusphere-2026-5337 (2026). Preprint.

43. Jourdain, N. C. *et al.* A protocol for calculating basal melt rates in the ISMIP6 Antarctic ice sheet projections. *The Cryosphere* **14**, 3111–3134, DOI: 10.5194/tc-14-3111-2020 (2020).

44. Dinniman, M. S. *et al.* Modeling ice shelf/ocean interaction in Antarctica: A review. *Oceanography* **29**, 144–153, DOI: 10.5670/oceanog.2016.106 (2016).

45. Galton-Fenzi, B. K., Hunter, J. R., Coleman, R., Marsland, S. J. & Warner, R. C. Modeling the basal melting and marine ice accretion of the Amery Ice Shelf. *J. Geophys. Res. Ocean.* **117**, DOI: 10.1029/2012jc008214 (2012).

46. Yung, C. K. *et al.* Results of the second Ice ShelfOcean Model Intercomparison Project (ISOMIP+). *The Cryosphere* **20**, 2053–2088, DOI: 10.5194/tc-20-2053-2026 (2026).

47. Gwyther, D. E., Dow, C. F., Jendersie, S., Gourmelen, N. & Galton-Fenzi, B. K. Subglacial Freshwater Drainage Increases Simulated Basal Melt of the Totten Ice Shelf. *Geophys. Res. Lett.* **50**, e2023GL103765, DOI: 10.1029/2023gl103765 (2023).

48. Papapetros, P., Galton-Fenzi, B. K., Gwyther, D. E., Boeira Dias, F. & Zhao, C. Effects of Sediment-Laden Subglacial Discharge on Ice Shelf Basal Melting and Seabed Evolution. *J. Geophys. Res. Ocean.* **130**, e2025JC023422, DOI: 10.1029/2025jc023422 (2025).

49. Nowicki, S., Payne, A. J. *et al.* The Ice Sheet Model Intercomparison Project for CMIP7 (ISMIP7): overview and protocol for standalone ice sheet models (2026). Manuscript in preparation.

50. Nowicki, S. *et al.* Experimental protocol for sea level projections from ISMIP6 stand-alone ice sheet models. *The Cryosphere* **14**, 2331–2368, DOI: 10.5194/tc-14-2331-2020 (2020).

51. Rignot, E. *et al.* Four decades of Antarctic Ice Sheet mass balance from 1979–2017. *Proc. Natl. Acad. Sci.* **116**, 1095–1103, DOI: 10.1073/pnas.1812883116 (2019).

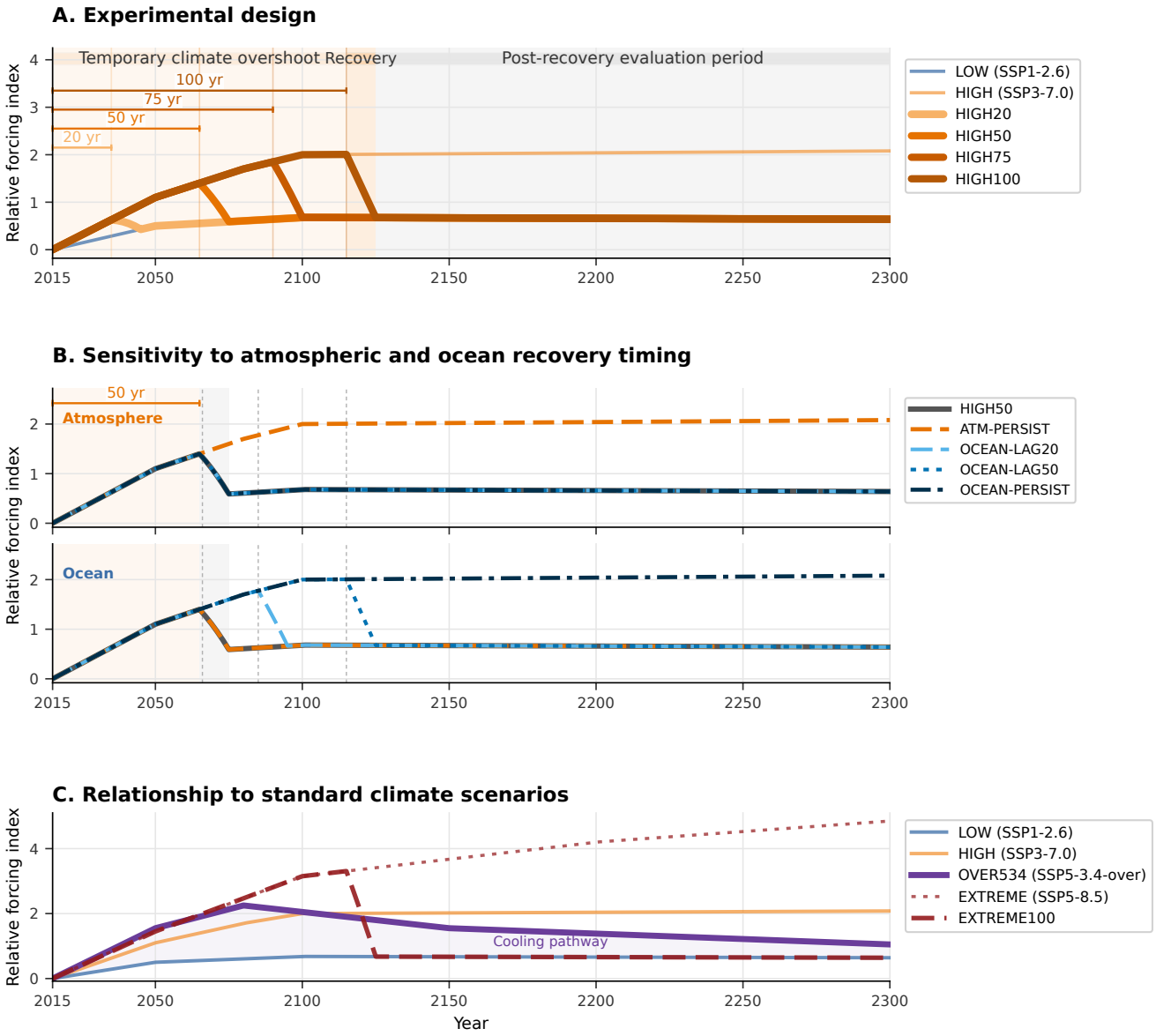


Figure 1. Schematic overview of the climate overshoot experiments. a, Schematic forcing pathways for the controlled climate overshoot experiments. The duration of elevated forcing (20, 50, 75 and 100 years) is systematically varied while maintaining an identical recovery pathway to isolate the effect of forcing duration on Antarctic sea-level contribution (ASC). LOW and HIGH denote the low- and sustained high-forcing reference experiments, respectively. **b**, Sensitivity experiments that isolate the effects of atmospheric and ocean recovery timing using HIGH50 as the control experiment. Atmospheric and ocean forcing are modified independently while all other aspects of the forcing remain unchanged. **c**, Relationship between the idealised experiments and the SSP5-3.4-over overshoot pathway (OVER534), together with the sustained high-forcing SSP3-7.0 (HIGH) and SSP5-8.5 (EXTREME) reference scenarios. Curves schematically illustrate the prescribed forcing histories; the experiments use spatially resolved climate fields. The relative forcing index is a schematic representation of the prescribed pathways, not a temperature scale or model output. In particular, the labelled durations indicate years of high forcing before recovery begins, not years above a 1.5 °C global-warming threshold.

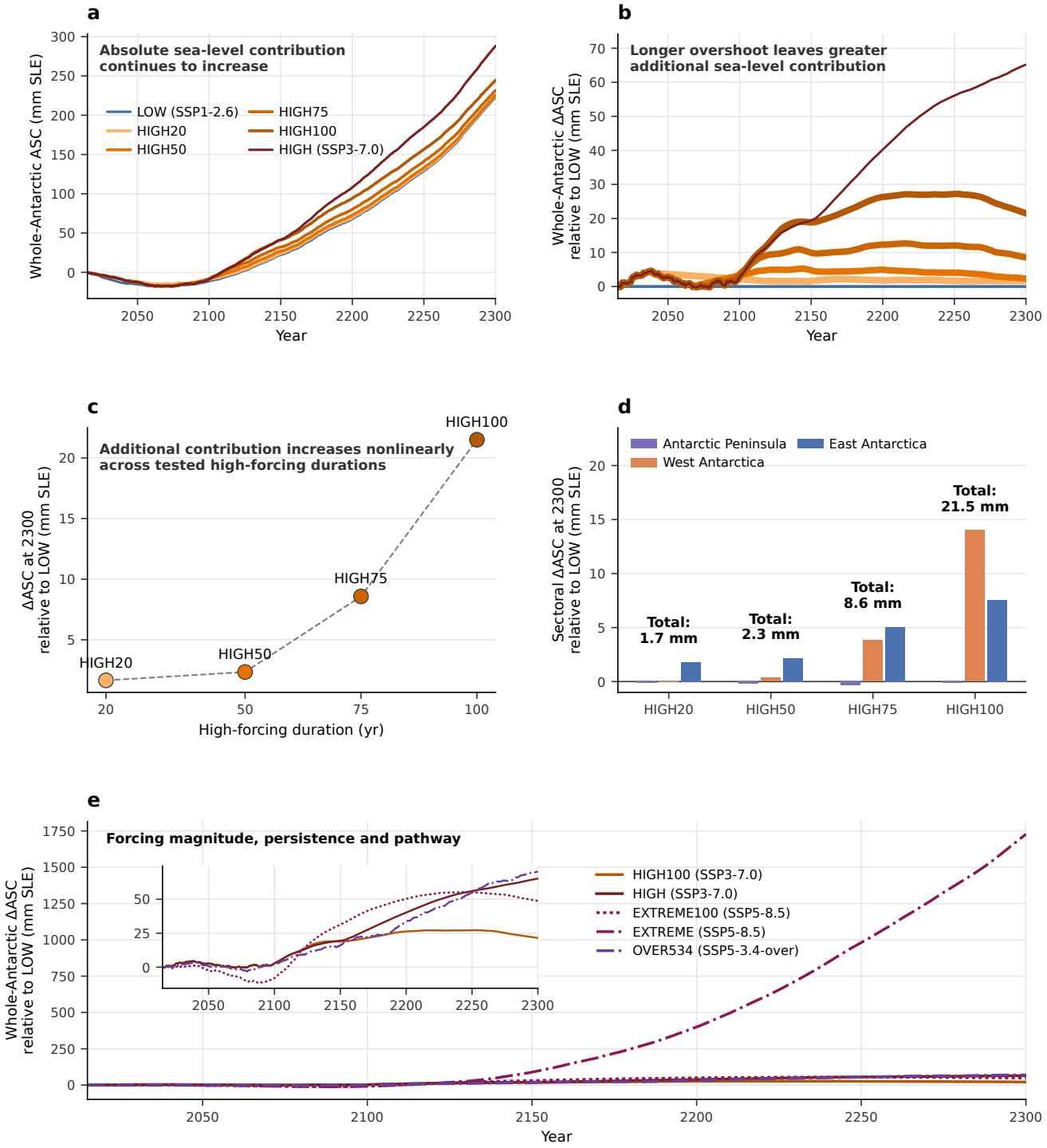


Figure 2. Antarctic sea-level contribution depends on high-forcing duration, magnitude and recovery pathway. a, Time series of cumulative whole-Antarctic sea-level contribution (ASC) under LOW (SSP1-2.6), the four temporary overshoot experiments (HIGH20, HIGH50, HIGH75 and HIGH100), and sustained HIGH (SSP3-7.0). **b,** Additional Antarctic sea-level contribution relative to LOW (ΔASC) for the same experiments. **c,** ΔASC at 2300 versus high-forcing duration. The dashed line connects discrete experiments as a visual guide. **d,** Contributions from East Antarctica (EAIS), West Antarctica (WAIS), and the Antarctic Peninsula (AP) to ΔASC at 2300. Labels show whole-Antarctic totals. **e,** ΔASC under HIGH100, sustained HIGH, EXTREME100, sustained EXTREME and OVER534. HIGH100 and EXTREME100 apply SSP3-7.0- and SSP5-8.5-derived forcing, respectively, for 100 years before a 10-year transition towards LOW; HIGH and EXTREME maintain their respective forcing pathways through 2300. OVER534 uses SSP5-3.4-over-derived climate forcing. The inset enlarges the four trajectories excluding sustained EXTREME. All sea-level contributions are expressed in millimetres of sea-level equivalent (mm SLE).

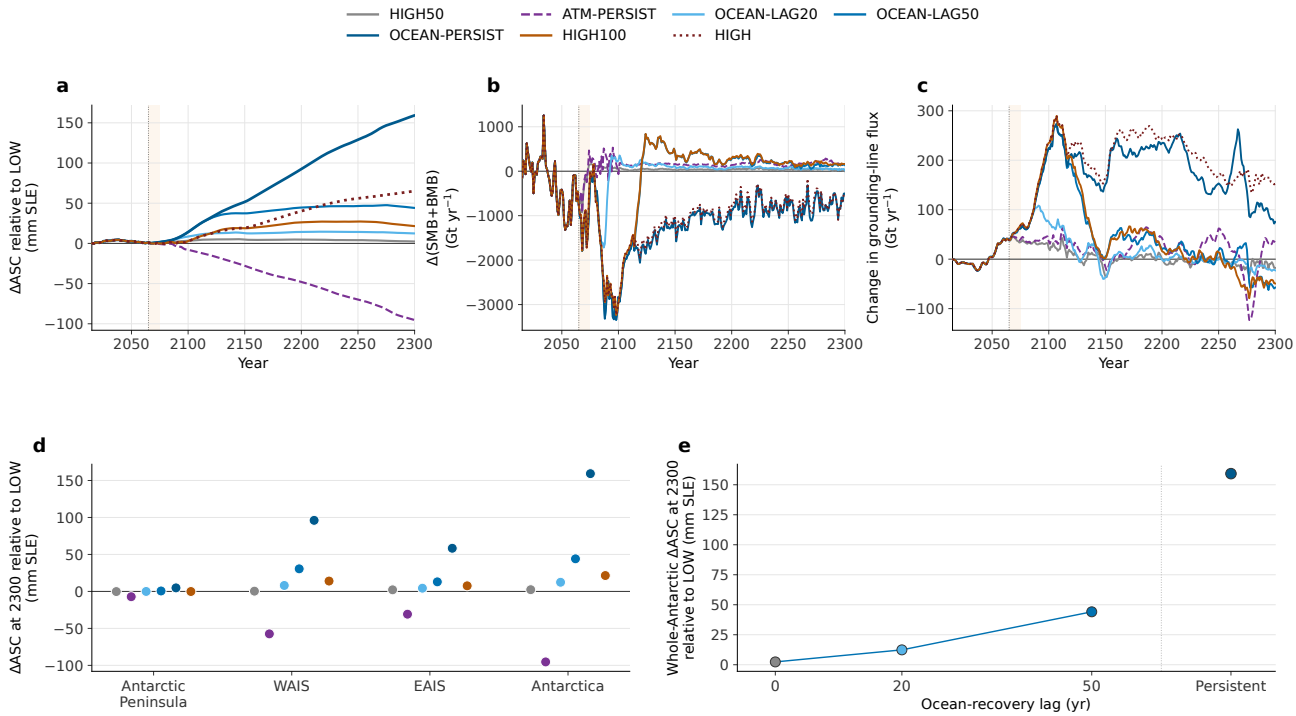


Figure 3. Ocean-forcing persistence and additional Antarctic sea-level contribution. **a**, Whole-Antarctic sea-level contribution relative to LOW (ΔASC) for HIGH50, ATM-PERSIST, OCEAN-LAG20, OCEAN-LAG50, OCEAN-PERSIST, HIGH100 and sustained HIGH. Experiment definitions are given in Table 1. **b**, Whole-Antarctic anomaly in the sum of surface and basal mass balance (SMB+BMB) relative to LOW. **c**, Whole-Antarctic anomaly in the area-integrated, model-exported grounding-line flux diagnostic relative to LOW. The diagnostics in **b** and **c** provide process context but do not include all terms governing changes in grounded ice above flotation and should not be summed to reconstruct ΔASC. **d**, ΔASC in 2300 for the Antarctic Peninsula, West Antarctic Ice Sheet (WAIS), East Antarctic Ice Sheet (EAIS) and total Antarctica; sustained HIGH is not shown. **e**, Whole-Antarctic ΔASC in 2300 by ocean-recovery lag. The line joining the finite-lag experiments (0, 20 and 50 years) is a visual guide; persistent ocean forcing is shown as a separate categorical endpoint. In the time-series panels, the vertical dotted line marks the start of recovery in HIGH50 in 2065, and shading marks its 10-year recovery period. Sea-level contributions are in mm sea-level equivalent (SLE), and fluxes are in Gt yr^{-1}.

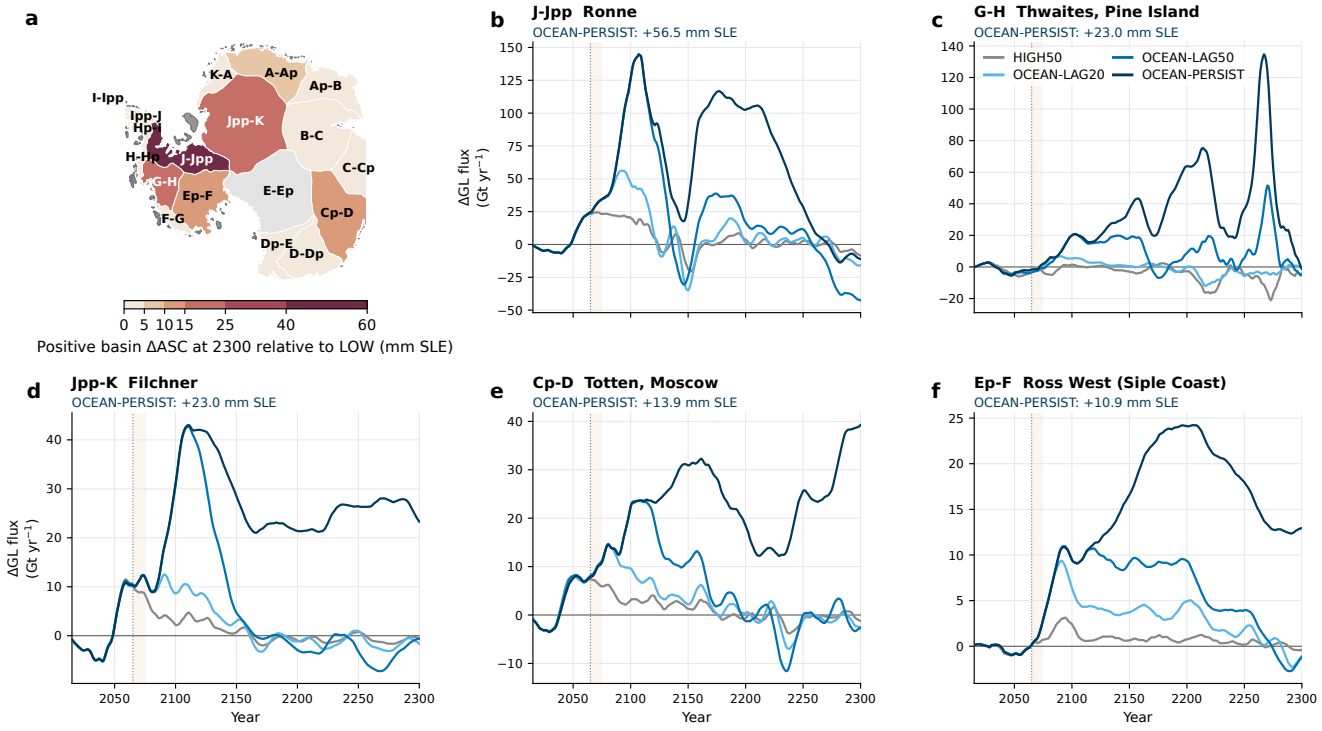


Figure 4. Basin-scale sea-level contribution and grounding-line-flux response to delayed ocean recovery. a, Basin ΔASC at 2300 under OCEAN-PERSIST relative to LOW. Warm colours show positive contributions using discrete intervals, and nonpositive values are shown in grey. **b–f**, Grounding-line-flux diagnostic relative to LOW for the five basins with the largest positive ΔASC: **b**, J–Jpp; **c**, G–H; **d**, Jpp–K; **e**, Cp–D; and **f**, Ep–F. Curves show centred 11-year running means for HIGH50, OCEAN-LAG20, OCEAN-LAG50 and OCEAN-PERSIST. The vertical dotted line marks the end of the common 50-year high-forcing period in 2065, and shading marks the subsequent 10-year transition. Positive values indicate greater grounding-line flux than under LOW. The grounding-line-flux diagnostic is not a closed basin mass budget.

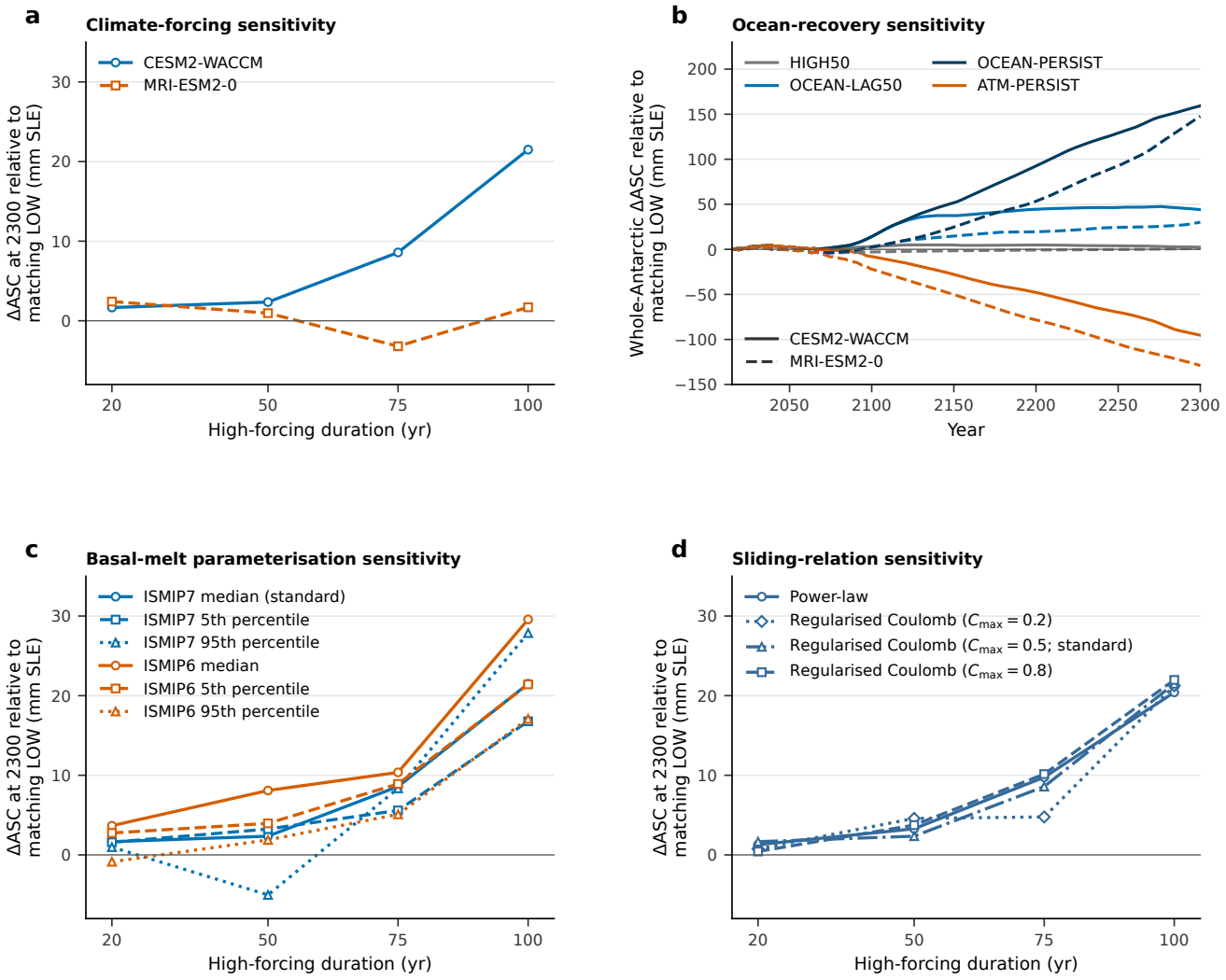


Figure 5. Sensitivity of Antarctic additional sea-level contribution to climate forcing and model configuration. a, Additional Antarctic sea-level contribution (ΔASC) at 2300 versus high-forcing duration under CESM2-WACCM and MRI-ESM2-0 climate forcing. **b**, Time series of whole-Antarctic ΔASC under synchronous atmospheric and ocean recovery (HIGH50), a 50-year delay in ocean recovery (OCEAN-LAG50), persistent high ocean forcing (OCEAN-PERSIST), and persistent high atmospheric forcing (ATM-PERSIST). Colours identify the recovery experiments; solid and dashed lines denote CESM2-WACCM and MRI-ESM2-0 forcing, respectively. **c**, ΔASC at 2300 versus high-forcing duration across the median, 5th-percentile and 95th-percentile calibrations of the ISMIP7 and ISMIP6 basal-melt parameterisations. The ISMIP7 median calibration is the standard configuration. **d**, ΔASC at 2300 versus high-forcing duration under the power-law sliding relation and regularised Coulomb relations with $C_{max} = 0.2$, 0.5 and 0.8; $C_{max} = 0.5$ is the standard configuration. All contributions are relative to the corresponding continuously low-forcing simulation and expressed in millimetres of sea-level equivalent (mm SLE). Lines in **a**, **c** and **d** connect discrete experiments as visual guides. These panels share the same y-axis range; **b** uses a wider range.

Supplementary Files

This is a list of supplementary files associated with this preprint. Click to download.

- SMAISovershoot.pdf